JOURNAL OF SOLID STATE CHEMISTRY 83, 304–315 (1989)

X-Ray Diffraction Study of Microstructure of Amorphous Tungsten Trioxide Films Prepared by Electron Beam Vacuum Evaporation

TOKURO NANBA AND ITARU YASUI

Institute of Industrial Science, University of Tokyo, Roppongi 7-22-1, Minato-ku, Tokyo, Japan 106

Received April 14, 1989; in revised form August 3, 1989

Microstructure of a-WO_3 films prepared by electron beam vacuum evaporation was examined based on XRD. The peak positions in the observed PDFs corresponded with those in the PDFs calculated from the crystal structure of hexagonal WO_3 and $WO_3 \cdot \frac{1}{3}H_2O$, and the framework structure of the films was therefore thought to consist of the basic structure of these crystals, three-, four-, and six-membered rings formed by WO_6 octahedra. Microcluster models in which the atomic arrangement was similar to that of hexagonal WO_3 were assumed and investigated in detail. The pair distribution functions calculated from these models showed good agreement with the observed values, and the structure of a-WO_3 films was consequently suggested to consist of clusters in which the octahedra were arranged in the same manner as those in hexagonal WO_3. © 1989 Academic Press, Inc.

Introduction

Amorphous tungsten trioxide (a-WO_3) films show electrochromic and photochromic properties and have been extensively studied in recent years. Microstructure of a-WO_3 films has been thought to consist of microclusters, and several structural models have been suggested. Zeller and Beyeler (*1*) investigated with XRD and concluded that WO_6 octahedra formed three- to six-membered rings sharing their corners. Kaito *et al.* (*2, 3*) suggested from TEM observation that microcrystallites with sizes 10 ~ 30 Å composed the film. Ramans *et al.* (*4–6*) claimed from Raman spectroscopy and XRD that the film involved terminal W=O bonds and consisted of clusters formed by three to eight WO_6 octahedra, each sharing its corners and edges. They also suggested a layered structure which was similar to those found in $MoO_3 \cdot 2H_2O$ crystal. Arnoldussen (*7*) suggested that trimeric W_3O_9 molecules were bound weakly to each other through water-bridge, hydrogen, and van der Waals bonding and that they constructed the film. The authors (*8*) suggested a microparticle structure but did not consider the presence of involved water. In this study, we analyzed the composition of a-WO_3 film and investigated microstructure in further detail based on pair distribution function (PDF) which was obtained with a new technique for XRD measurement.

Experimental

WO_3 film specimens were prepared by Asahi Glass Co., Ltd., with electron beam vacuum evaporation using Model EVD-500B (Anelva). WO_3 powder preheated at

0022-4596/89 $3.00

TABLE I

CONDITIONS OF THE SAMPLE PREPARATION, THICKNESS, AND DENSITY OF THE PREPARED a-WO_3 FILMS FOR XRD MEASUREMENT

Sample no.	Ts[a] (°C)	Ta[b] (°C)	Thickness (Å)	Density (g/cm^3)
1	RT	—	8000	4.09
2	150	—	7700	4.45
3	300	—	4400	5.40
4	RT	300	7200	4.60

[a] Substrate temperature.
[b] Annealing temperature.

700°C for 6 hr was used as a source and deposited onto a soda-lime glass substrate under 4×10^{-4} Torr pressure and at different substrate temperatures Ts = RT, 150, and 300°C. We examined the composition of the prepared films. The ratio of oxide-oxygen to tungsten was estimated with ESCA. The quantity of the involved water was determined with the results of thermogravimetry (TG) and FTIR. The total weight of W atom present in a film was estimated from fluorescent X-ray analysis, and density was determined through a combination of weight of W, film composition, and thickness measured with Talystep. The thicknesses and densities of the films for XRD measurements are listed in Table I. XRD measurements were carried out using Rigaku-Denki Rota-Flex RU-200 equipped with a thin film diffractometer (TFD). The size of the specimen was 2×2 cm, and the incident beam angle was selected as 2°. A Mo$K\alpha$ radiation with an output of 60 kV–150 mA was monochromatized with a pair of balanced filters (Zr–Y) and a graphite monochromator in a diffracted beam along with a pulse height analyzer. After some of the data corrections (*9, 10*), we obtained PDF. Structural models were constructed based on crystalline tungsten oxides.

TABLE II

ANALYZED COMPOSITION OF a-WO_3 FILMS

Sample no.	O_{ox}/W (oxide)	O_{hy}/W (hydrate)	O_{tot}/W (total)
1	2.8	1.0	3.8
2	2.9	0.7	3.6
3	3.1	0.5	3.6
4	3.0	0.2	3.2

Results

1. Compositions of a-WO_3 Films

The analyzed compositions are listed in Table II. The atomic ratio, oxide-oxygen to tungsten O_{ox}/W, was estimated from the peak area of O_{1s} and W_{4f} in ESCA measurement. It was very difficult to determine the exact quantity of oxygen, because oxygen atoms in the films were easily removed by an ion bombardment in pretreatment. We therefore worked out a correction curve from the results for some crystalline tungsten oxides (*11*), and we determined the ratio accordingly. The estimated ratios of our films were smaller than 3.0 except for the sample 3 (Ts = 300°C).

Quantity of the involved water was estimated as the atomic ratio hydrate-oxygen to tungsten O_{hy}/W with a combination of TG and FTIR spectra. In the result of TG, two steps of small weight loss were observed at about ~150 and ~300°C, and both were assigned to the dehydration of waters involved in the films. Similar result was reported by Zeller and Beyeler (*1*) from DSC and TG analyses. The weight of the specimen used in the TG measurement was too small to give an accurate quantity of water, and we therefore referred to the results of FTIR reported by Shigesato *et al.* (*12*). They prepared a-WO_3 films on Si single crystals with the same method and conditions. We determined the relative values of the O_{hy}/W ratios from the peak area around 3300 cm^{-1}.

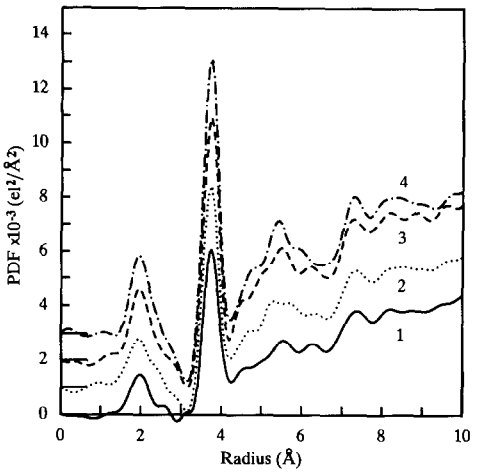

FIG. 1. Observed PDFs for a-WO_3 films prepared under the different conditions. Solid line, sample 1 (Ts = RT, Ta = none); dotted line, sample 2 (Ts = 150°C, Ta = none); broken line, sample 3 (Ts = 300°C, Ta = none); chain, sample 4 (Ts = RT, Ta = 300°C).

As Ts becomes higher, the O_{ox}/W ratio increases and the O_{hy}/W ratio decreases as shown in Table II. The O_{ox}/W ratio of the annealed film (Ta = 300°C) was not so different from that of Ts = 300°C, but the O_{hy}/W ratio was found to be much smaller ($\approx\frac{1}{3}$). The residual gas in the vacuum chamber contained more than 90 wt% of water, which was estimated by mass spectrometer. We therefore thought that the origin of most of the involved water was in the vapor phase, and, at higher Ts, water in the film was easily evaporated and the final water content was consequently lowered.

2. *Pair Distribution Functions*

The obtained PDFs are shown in Fig. 1. Two main peaks can be observed near 2 and 4 Å. The first peaks at about 2 Å are assigned to the nearest neighboring W–O pairs and the second peaks at 4 Å are assigned mainly to the nearest W–W pairs. The first peaks in every PDF are broad, which suggests the distance between the nearest W–O is widely distributed. On the contrary, the second peak is considerably sharp. We therefore concluded that the shape of the octahedra consisting of WO_6 or $WO_{6-x}(OH_2)_x$ was distorted but that the mode of the connection between these octahedra was in rather good order. The other peaks observed at over 4 Å consisted of complicated peaks but the PDF showed some details even at 10 Å. We investigated the coordination number (Nco) of the nearest W–O and W–W from the first and second peaks. The second peak consisted of not only W–W (3.7 Å) but also the second nearest W–O (4 Å). The contribution of W–O was estimated to be about 15% of the total PDF at 3.7 Å, which was in the case of some crystalline tungsten oxides. The results are shown in Table III. It was found that the Nco for W–O and W–W increased as both Ts and Ta became higher. The Nco(W–O) values were less than 6 for samples 1 and 2. This is explained by the coexistence of WO_4 tetrahedra and WO_6 octahedra, which have not been reported for a-WO_3 film. These samples contained much water and the shoulders around 2.4 Å in PDF were attributed to the bonds W–OH_2 (2.1 ~ 2.3 Å) in the octahedra $WO_{6-x}(OH_2)_x$. This assumption gives an account of the apparent lack of Nco(W–O).

Discussion

1. *Comparison with the Crystal Structures in PDF*

We calculated PDFs from several crystalline tungsten oxides and their hydrates

TABLE III

COORDINATION NUMBER OF THE NEAREST W–O AND W–W OF a-WO_3 FILMS

Sample	W–O	W–W
1	(4.5)	4.3
2	(5.5)	4.6
3	6.0	5.1
4	6.0	5.3

TABLE IV

STRUCTURAL DATA OF CRYSTALLINE TUNGSTEN OXIDES AND HYDRATES

Crystal	Space group	Lattice constant a	b	c (Å)		Density[a] (g/cm³)	Ref.
1. ReO_3-type							
monoclinic WO_3	$P2_1/a$	7.27	7.50	3.82	$\beta = 89.9°$	7.38	*13*
tetragonal WO_3	$P4/nmm$	5.27		3.92		7.14	*13*
2. Substoichiometric							
$W_{18}O_{49}$	$P2/m$	18.32	3.79	14.04	$\beta = 115.2°$	7.71	*13*
$W_{20}O_{58}$	$P2/m$	12.05	3.77	23.49	$\beta = 85.3°$	7.17	*13*
3. Layered							
$MoO_3 \cdot 2H_2O$[b]	$P2_1/n$	10.48	13.82	10.61	$\beta = 91.6°$	4.64	*14*
$WO_3 \cdot H_2O$	$Pnmb$	5.25	10.71	5.13		5.75	*15*
4. Six-membered ring							
hexagonal WO_3	$P6/mmm$	7.30		7.80	$\gamma = 120.0°$	6.43	*16*
$WO_3 \cdot \frac{1}{3}H_2O$	$Fmm2$	7.36	12.51	7.70		6.68	*17*

[a] Calculated density.

[b] The structural parameters of $WO_3 \cdot 2H_2O$ have not been given; hence the data of $MoO_3 \cdot 2H_2O$ are listed. The density was calculated by substituting Mo for W.

and compared them with the observed PDFs. We chose eight crystals and divided them into four groups as listed in Table IV. The first group is formed by monoclinic and tetragonal WO_3, which are polymorphic forms in ReO_3-type structure. The second group consists of substoichiometric oxides WO_{3-x} containing edge-sharing octahedra. The third group contains molybdenum and tungsten oxide hydrates which have a layered structure. The last two crystals in the fourth group, hexagonal WO_3 and $WO_3 \cdot \frac{1}{3}H_2O$, are produced by dehydration of tungsten oxide hydrates, and they consist of three-, four-, and six-membered rings formed by WO_6 octahedra (*16, 17*).

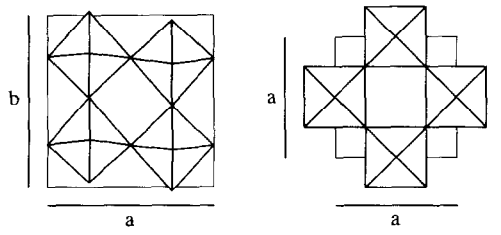

(a) monoclinic WO_3 (b) tetragonal WO_3

FIG. 2. Crystal structures of (a) monoclinic and (b) tetragonal WO_3 with ReO_3-type structure.

The first group, monoclinic and tetragonal WO_3, can be described as a distorted cubic structure of the ReO_3 type. The structure of these crystals is illustrated in Fig. 2, in which the lines exhibit the edges of WO_6 octahedra to explain the configuration of the octahedra. The calculated PDFs from these crystals, which are compared with the observed PDF of sample 3, are shown in Fig. 3. The WO_6 octahedra in monoclinic WO_3 are distorted and the bond length of W–O is widely distributed between 1.5 to 2.3 Å; hence, the first peak becomes broad in PDF. But the areas of the first peaks for both crystals are much the same as that of sample 3, which indicates the Nco(W–O) of the film is 6. The second peaks for these crystals are located at slightly longer positions than that of our samples. Large third or fourth peaks, which are mainly attributed to W–W on the opposite corners in the

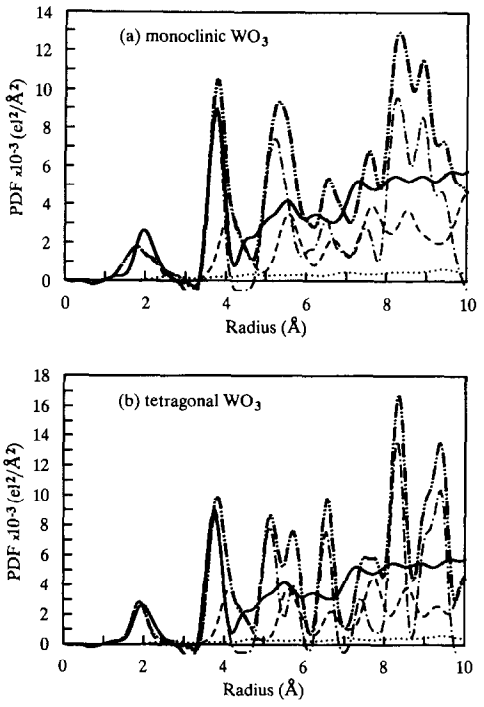

FIG. 3. Calculated PDFs from (a) monoclinic and (b) tetragonal WO_3. Solid line, observed PDF of sample 3; dotted line, O–O; broken line, W–O; single chain, W–W; double chain, sum of each pair.

four-membered rings, appear around 5 ~ 6 Å. The observed PDFs, on the other hand, show broad and weak peaks in this region.

In the substoichiometric tungsten oxides, $W_{18}O_{49}$ ($WO_{2.72}$) and $W_{20}O_{58}$ ($WO_{2.90}$), the shortage of oxygen is compensated by formation of the edge-sharing octahedra, which is shown in Fig. 4, and a channel structure stabilizes this structure. The distances between the nearest W–W are widely distributed in these crystals, and the second peak in PDFs hence become broad (Fig. 5). The third peaks are very strong, which is the same as those of the previous two WO_3 crystals. These results suggested that the edge-sharing structures were not present in our films as much as detectable.

The accurate structural parameters of $WO_3 \cdot 2H_2O$ in the third group have not been given, but tungsten oxide hydrates are commonly thought to have a structure similar to molybdenum oxide hydrates. For example, the atomic arrangement of $WO_3 \cdot H_2O$ (*15*) is similar to that of $MoO_3 \cdot H_2O$ (*18*). We accordingly assumed that the

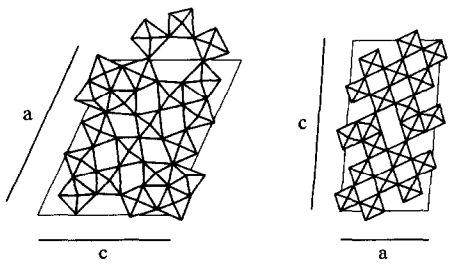

FIG. 4. Crystal structures of substoichiometric tungsten oxides, (a) $W_{18}O_{49}$ and (b) $W_{20}O_{58}$.

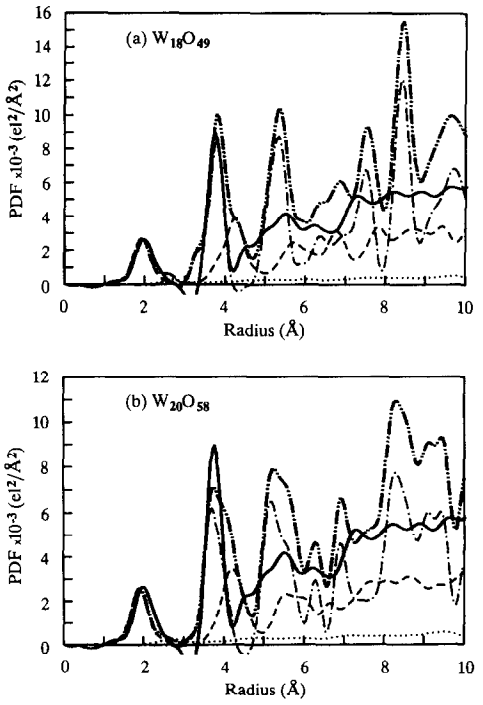

FIG. 5. Calculated PDFs from (a) $W_{18}O_{49}$ and (b) $W_{20}O_{58}$. Solid line, observed PDF of sample 3; dotted line, O–O; broken line, W–O; single chain, W–W; double chain, sum of each pair.

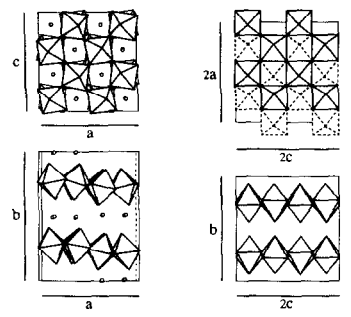

FIG. 6. Crystal structures of (a) $MoO_3 \cdot 2H_2O$ and (b) $WO_3 \cdot H_2O$ taking a layered structure. The solid and broken lines exhibit the edges of MoO_6 and WO_6 octahedra and the circles are oxygen atoms in the isolated water molecules.

structure of $WO_3 \cdot 2H_2O$ was the same as that of $MoO_3 \cdot 2H_2O$ and calculated PDF with the structural parameters of $MoO_3 \cdot 2H_2O$ (*14*). In the above-mentioned hydrates, the octahedra are arranged in infinite layers as illustrated in Fig. 6, and one W or Mo is octahedrally coordinated by four bridging O, one terminal O, and one O in a water molecule. In addition to coordinating water molecules, $MoO_3 \cdot 2H_2O$ contains isolated water molecules between the layers, which have hydrogen bonds with the neighboring layers. The calculated PDFs from these hydrates are shown in Fig. 7. The Nco(W–W) or (Mo–Mo) is 4 in both hydrates and the areas of the second peaks in the calculated PDFs are smaller than that of the observed PDF. These hydrates have layered structure and no W–O–W bonds in the direction parallel to the *b*-axis, and the peak area is therefore insufficient in the region between 3.5 to 7.0 Å, which can be seen clearly in the case of $WO_3 \cdot 2H_2O$.

In the last group, the structures of hexagonal WO_3 and $WO_3 \cdot \frac{1}{3}H_2O$ have been reported by Gerand *et al.* (*16, 17*). The hexagonal type is a new form of WO_3, and WO_6 octahedra are arranged in the manner of not only four-membered rings but also three- and six-membered rings sharing their corners (Fig. 8a). It can be obtained by dehydration of $WO_3 \cdot \frac{1}{3}H_2O$ (Fig. 8b), which is prepared by hydrothermal treatment of an aqueous suspension of either tungstic acid gel or crystallized $WO_3 \cdot 2H_2O$. The arrangement of the octahedra is similar to that of hexagonal WO_3 in the layer perpendicular to the *c*-axis. The calculated peaks appeared at places corresponding with those of our films as shown in Fig. 9. The average distances of W–W are 3.7, 6.3, and 7.3 Å in the six-membered rings and 5.3 Å in the four-membered rings in hexagonal WO_3. The six-membered rings are also observed in substoichiometric WO_3 but the distances of the nearest W–W had wider

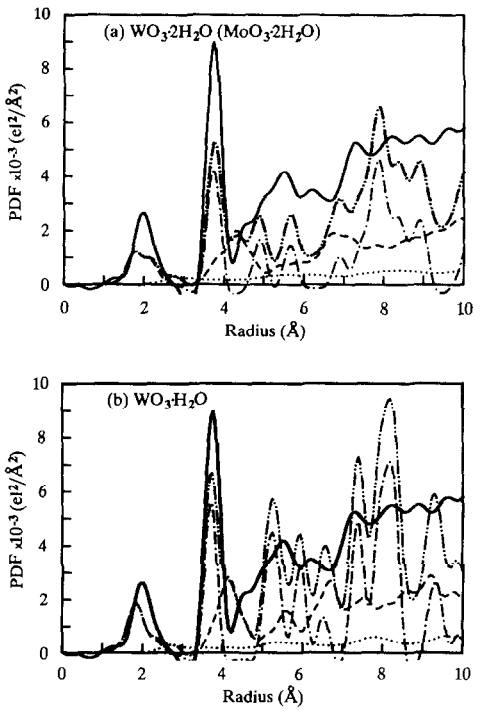

FIG. 7. Calculated PDFs from (a) $WO_3 \cdot 2H_2O$ and (b) $WO_3 \cdot H_2O$. The PDF of $WO_3 \cdot 2H_2O$ was calculated with the structural parameters of $MoO_3 \cdot 2H_2O$ (*14*). Solid line, observed PDF of sample 3; dotted line, O–O; broken line, W–O; single chain, W–W; double chain, sum of each pair.

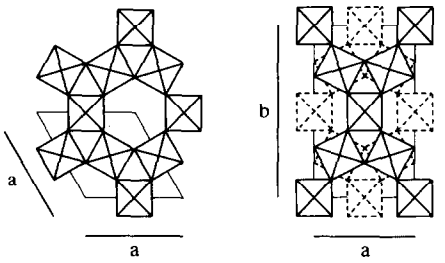

FIG. 8. Crystal structures of (a) hexagonal WO_3 and (b) $WO_3 \cdot \frac{1}{3}H_2O$ containing three- and six-membered rings formed by WO_6 octahedra.

distributions. Two kinds of octahedra are present in $WO_3 \cdot \frac{1}{3}H_2O$. One is formed by six bridging O and the other is formed by four bridging O, one terminal O, and one O from water, which is the same as the previously discussed third group hydrates. However, hexagonal WO_3 and $WO_3 \cdot \frac{1}{3}H_2O$ have no layered structures and the areas in the region around 5 ~ 6 Å were greater than those of the previously discussed hydrates. Large peaks appeared at about 7.3 Å, which are consistent with the observed peak.

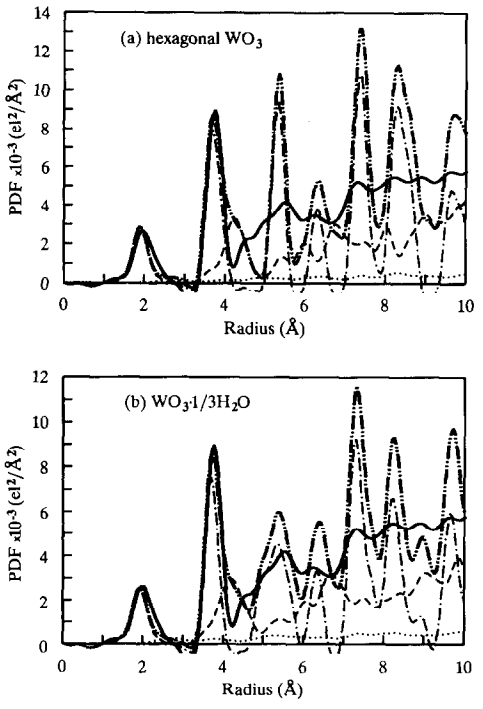

FIG. 9. Calculated PDFs from (a) hexagonal WO_3 and (b) $WO_3 \cdot \frac{1}{3}H_2O$. Solid line, observed PDF of sample 3; dotted line, O–O; broken line, W–O; single chain, W–W, double chain, sum of each pair.

From these examinations, it was found that the positions of the first and second peaks in the observed PDFs were consistent with all of the calculated PDFs for the compared crystals. However, the areas of the second peaks were deficient in the hydrates of the third group, and we therefore thought that our films did not consist of the simple layered structures. The peak positions in the region over 4 Å were somewhat different among the examined crystals, which was due to the difference in the configuration of the network formed by WO_6 octahedra. The peaks commonly observed around 5 ~ 6 Å were mainly attributed to the W–W pairs located at opposite corners in the four-membered rings and the second neighbors in the six-membered ones. Large characteristic peaks commonly appeared at 7.3 Å in the observed PDFs, and these peaks could not be observed except for hexagonal WO_3 and $WO_3 \cdot \frac{1}{3}H_2O$. In addition to this, even the small peaks in the observed PDFs were consistent with the peaks of hexagonal WO_3 and $WO_3 \cdot \frac{1}{3}H_2O$. We therefore expected that the framework structure of a-WO_3 films was similar to that of hexagonal WO_3 and $WO_3 \cdot \frac{1}{3}H_2O$, which was based on three-, four-, and six-membered rings formed by WO_6 octahedra.

2. *Structural Models*

We obtained the best agreement between the PDFs of our films and those of hexagonal WO_3 and $WO_3 \cdot \frac{1}{3}H_2O$. Then we made some cluster models based on the structure of these crystals and examined them. At first, we calculated Nco(W–W) to compare with those of our films. We constructed

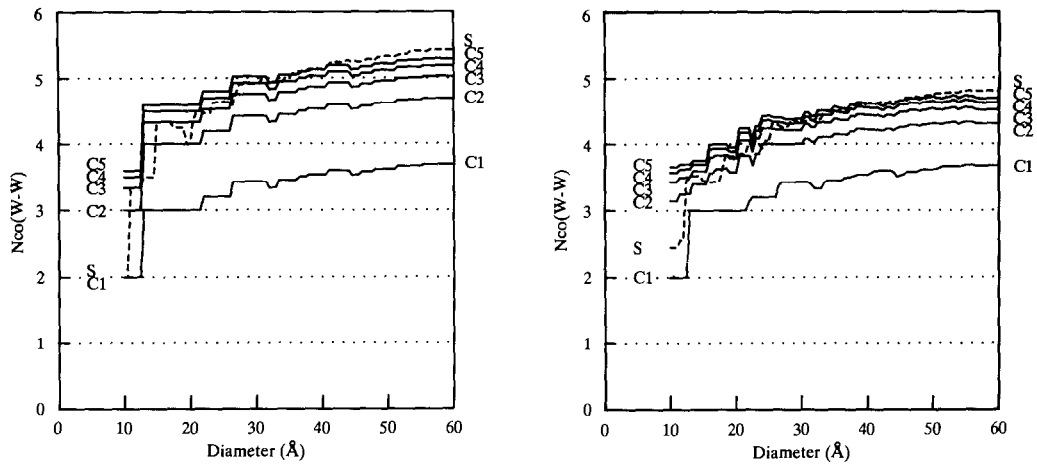

FIG. 10. Coordination number (Nco) of the nearest W–W in the microclusters based on the atomic arrangement of (a) hexagonal WO_3 and (b) $WO_3 \cdot \frac{1}{3}H_2O$ crystals. S and C indicate spherical and columnar clusters, respectively, and the digits following exhibit the number of WO_6 octahedra linked in vertical direction.

cluster models with spherical and columnar shape. The atoms were arranged in spherical and columnar form of a unit cell in which the Nco(W–W) became as big as possible. As shown in Fig. 10, the calculated Nco(W–W) values from hexagonal WO_3 were bigger than those from $WO_3 \cdot \frac{1}{3}H_2O$ in the same diameter. The Nco(W–W) values of our films were estimated to be 4.3 ~ 5.3, and we consequently chose the same configuration of WO_6 octahedra as hexagonal WO_3. The columnar form was selected to simplify the arrangement of the cluster models.

However, the shape of the third peaks around 5 ~ 6 Å in the observed PDFs was similar to that of $WO_3 \cdot \frac{1}{3}H_2O$. The distances of W–W in this region are 5.3 Å in hexagonal WO_3 and 5.0, 5.3, and 5.6 Å in $WO_3 \cdot \frac{1}{3}H_2O$ so that the peaks of hexagonal WO_3 become sharper. The bond angles of W–O–W and O–W–O in the structural models were accordingly chosen to be the same as $WO_3 \cdot \frac{1}{3}H_2O$.

(1) Structural model for sample 1. At first we considered the size of the cluster model and the inner atomic arrangement. To satisfy the observed Nco(W–W) of 4.3, a cluster model 16 Å in diameter and 12 Å in thickness and with Nco(W–W) of 4.33 was selected. The model is illustrated in Fig. 11. The three- and six-membered rings are located on the projected X–Y plane and the

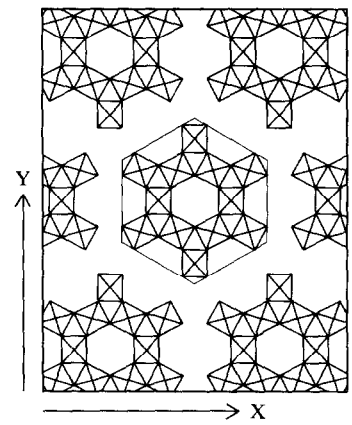

FIG. 11. Structural model of sample 1 projected along Z direction. The arrows indicate 20 Å.

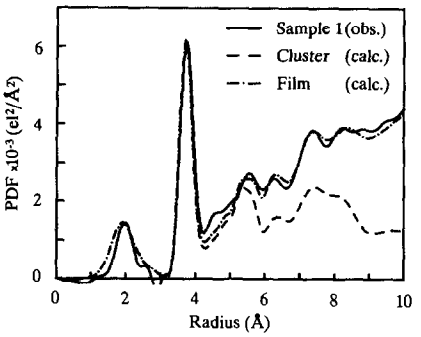

FIG. 12. Calculated PDF from the structural model of sample 1.

four-membered rings are parallel to the vertical Z direction. Three WO_6 octahedra are linked along the Z axis. The O_{tot}/W ratio of this model is 3.83 ($W_{36}O_{138}$), which is close to the observed ratio of 3.8. The calculated PDF from this cluster model (broken line in Fig. 12) showed good agreement with the observed value up to the second peaks.

Then we considered the arrangement of these clusters. The shape of the model is hexagonal plate, and the cluster models were therefore placed in positions similar to a hexagonal close packing. The distance between the clusters was calculated to be 2.46 Å to satisfy the observed density. The total PDF as a film (chain in Fig. 12) which included the interaction between the clusters showed good agreement with the observed value. We examined various arrangements of the clusters, but the effect did not appear clearly in PDF. We found that the peaks in the observed PDFs were mainly affected by the atomic arrangement in the clusters.

We tried to explain the presence of three- and six-membered rings on the basis of the evaporation process. The three-membered rings in the cluster were ascribed to the structure of trimeric W_3O_9 molecule in vapor phase which was reported by Berkowitz (*19*). The deposited W_3O_9 molecules are bound through water-bridging in the initial stage. The W–O bonds in the ring are unchanged and these molecules are tied together to form the six-membered ring.

(2) *Structural model for sample 2.* As for sample 2, the structural model as shown in Fig. 13 showed the best agreement in PDF (Fig. 14). The diameter of the cluster in this model is 30 Å, which is greater than that of sample 1, and the thickness in the Z direction is the same as that of the sample 1. The arrangement of the clusters is similar to that of sample 1, which has no direct bonds as W–O–W between the clusters. Although the Ts is higher than that for sample 1, the basic structure of this model is the same as that of sample 1 and the calculated PDF is

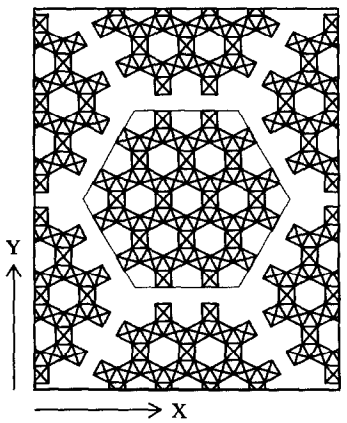

FIG. 13. Structural model of sample 2 projected along Z direction. The arrows indicate 20 Å.

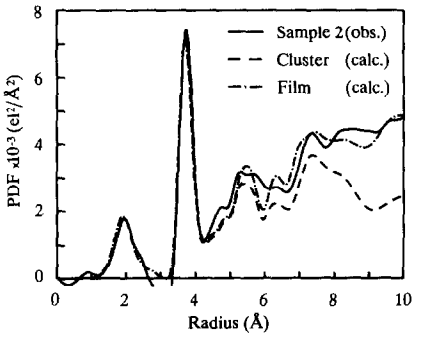

FIG. 14. Calculated PDF from the structural model of sample 2.

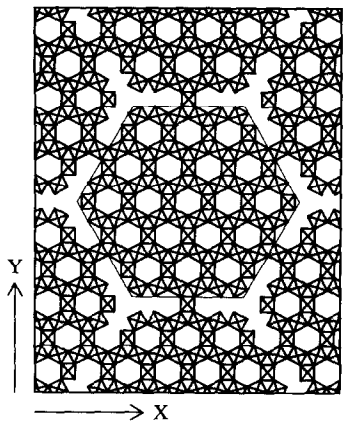

FIG. 15. Structural model of sample 3 projected along Z direction. The arrows indicate 20 Å.

quite consistent with the observed value. This result suggests that the three- and six-membered rings are fairly stable, but they disappear and only the four-membered rings are formed when Ts exceeds 360°C. Above that temperature WO_3 films will crystallize and form ReO_3-type structure.

(3) Structural model for sample 3. The observed density of this film was 5.4 g/cm^3, which was the highest in the four samples. When the clusters were arranged to have no direct bonds, the calculated distances between the clusters with desirable Nco (W–W) became too short. We therefore adopted a model in which the WO_6 octahedron was shared by the neighboring two clusters as shown in Fig. 15. The diameter and thickness of this cluster are 39 and 16 Å, respectively. The calculated PDF from this model is consistent with the observed value, which is shown in Fig. 16.

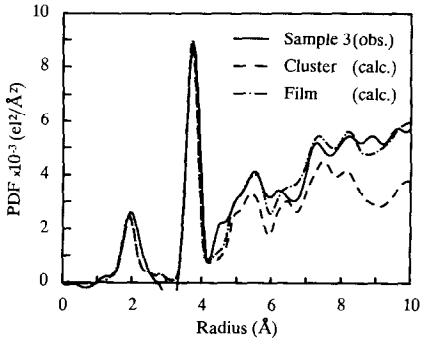

FIG. 16. Calculated PDF from the structural model of sample 3.

As the Ts became higher, the sizes of the clusters in these models increased. The clusters were isolated in samples 1 and 2 but they connected with each other in this model. This result seemed to reflect a structural change from the isolated clusters to a continuous structure.

(4) Structural model for sample 4. The density of this film was lower than that of sample 3, but the Nco(W–W) showed the greatest value, 5.3. This film was prepared by annealing of sample 1. We thought that samples 4 and 3 had different structures although both films were heated at 300°C. In sample 3, the deposited molecules or atoms can migrate to form microclusters. However, in sample 4, the clusters are already formed (in sample 1) and have a stable structure. The migration of the inner atoms may be considerably restricted in comparison with the case of sample 3. We therefore thought the clusters migrated and condensed through the heat treatment. We accordingly assumed a condensation of the clusters for sample 4. We made an infinite columnar model as shown in Fig. 17, which consisted of three of the clusters obtained for sample 1 in the projected X–Y plane. The columnar model had an infinite length in the vertical Z direction. Constructing this infinite columnar model, we satisfied the desirable density and Nco(W–W). The calculated PDFs which are consistent with the observed value, are shown in Fig. 18.

The specifications of the obtained structural models are listed in Table V.

From these studies, it was found that the structural models based on the atomic arrangement of hexagonal WO_3 showed good agreement in PDF. The framework structures in the cluster models consisted of

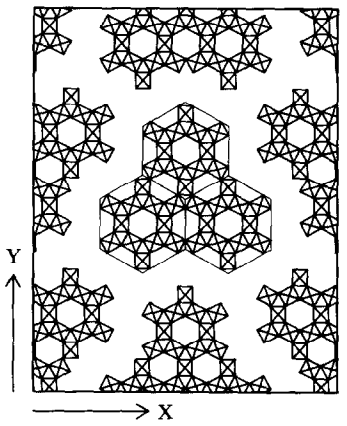

FIG. 17. Structural model of sample 4 projected along Z direction. The arrows indicate 20 Å.

three-, four-, and six-membered rings, and nonbridging oxygens in terminal W=O or $W-OH_2$ were located at the surface of the clusters. The structural changes, which were due to a rise of substrate temperature and annealing of a deposited film, were explainable by the growth of the clusters (sample 1 → 2 → 3) and condensation of the clusters (sample 1 → 4).

Information about the conformation of water can be obtained with IR spectra, but we did not reflect them to the structural models. This was based on the following reasons. The indicated cluster models were equal in size for each sample, but in fact the films probably consist of clusters with various sizes and shapes. We thought that the relation between such complicated clusters was much more complicated than the atomic configuration in the clusters. From these reasons, we made simple cluster models to explain basic structure and adjusted only the distances between the clusters. It is necessary to obtain more information on hydrogen in order to give a more detailed structure.

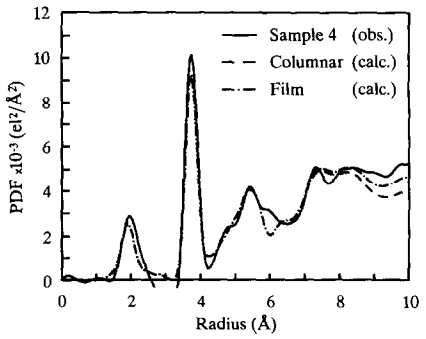

FIG. 18. Calculated PDF from the structural model of sample 4.

TABLE V

SPECIFICATION OF THE OBTAINED STRUCTURAL MODELS

Sample no.	Dc[a] (Å)	Tc[b] (Å)	N_W[c]	N_O[c]	O_{tot}/W	Nco (W–W)	Dc-c[d] (Å)
1	15.6	12.2	36	138	3.83	4.33	2.46
2	29.9	12.2	126	456	3.62	4.76	2.52
3	39.4	15.7	300	1023	3.41	5.18	2.50
4	15.6 × 3	∞	144	480	3.33	5.50	5.00

[a] Diameter of cluster.
[b] Thickness of cluster.
[c] Number of atoms in one cluster.
[d] Distance between clusters.

Conclusion

In this study, information about the microstructures of a-WO_3 films was obtained mainly with XRD using a TFD system. The second peaks attributed to the nearest W–W in PDFs were very sharp, and we accordingly expected that the configuration of WO_6 octahedra was kept in good order even over a long range. The observed PDFs were compared with the calculated values from crystalline tungsten oxides and hydrates, and they were consistent with the calculated PDFs from hexagonal WO_3 and $WO_3 \cdot \frac{1}{3}H_2O$. We therefore made cluster models based on the structure of these crystals. The clusters based on $WO_3 \cdot \frac{1}{3}H_2O$ required a considerably large size to satisfy the observed coordination number of the nearest W–W. The cluster models in which the atomic arrangement was similar to that

of hexagonal WO_3 showed good agreement in PDFs. The arrangement of the clusters did not have a pronounced effect on PDF, and it was not examined in detail. We thought the clusters in a-WO_3 film were bound to other clusters with hydrogen bonds through water molecules.

Acknowledgments

The authors thank Mr. T. Kamimori and Mr. Y. Shigesato of the Asahi Glass Co., Ltd., for their valuable suggestions and encouragement. We also thank the computer center, Institute for Molecular Science, Okazaki National Research Institutes, for the use of the HITAC M-680H and S820/20 computers.

References

1. H. R. Zeller and H. U. Beyeler, *Appl. Phys.* **13,** 231 (1977).
2. M. Shiojiri, T. Miyano, and C. Kaito, *Japan. J. Appl. Phys.* **17,** 567 (1978).
3. C. Kaito, T. Shimizu, Y. Nakata, and Y. Saito, *Japan. J. Appl. Phys.* **24,** 117 (1985).
4. G. M. Ramans, J. V. Gabrusenoks, and A. A. Veispals, *Phys. Status Solidi* **74,** K41 (1982).
5. J. V. Gabrusenoks, P. D. Cikmach, A. R. Lusis, J. J. Kleperis, and G. M. Ramans, *Solid State Ionics* **14,** 25 (1984).
6. G. M. Ramans, J. V. Gabrusenoks, A. R. Lusis, and A. A. Patmalnieks, *J. Non-Cryst. Solids* **90,** 637 (1987).
7. T. C. Arnoldussen, *J. Electrochem. Soc.* **128,** 117 (1981).
8. T. Nanba and I. Yasui, *Diffus. Data* **53–54,** 105 (1987).
9. I. Yasui and T. Nanba, *Diffus. Defect. Data* **53–54,** 439 (1987).
10. T. Nanba and I. Yasui, *Anal. Sci.* **5,** 257 (1989).
11. K. Kawakami, E. Ando, K. Matsuhiro, K. Matsumoto, M. Sugizaki, and H. Nishimura, *Rep. Res. Lab. Asahi Glass Co., Ltd.* **33** (1983).
12. Y. Shigesato, A. Maruyama, T. Kamimori, and K. Matsuhirio, *Appl. Surf. Sci.* **33–34,** 804 (1988).
13. R. W. G. Wycoff, "Crystal Structures," 2nd ed., Chap. VB, Wiley, New York (1964).
14. V. B. Krebs, *Acta Crystallogr. Sect. B* **28,** 2222 (1972).
15. J. T. Szymanski and A. C. Roberts, *Canad. Mineral.* **22,** 681 (1984).
16. B. Gerand, G. Nowogrocki, J. Guenot, and M. Figlarz, *J. Solid State Chem.* **29,** 429 (1979).
17. B. Gerand, G. Nowogrocki, and M. Figlarz, *J. Solid State Chem.* **38,** 312 (1981).
18. J. R. Gunter, *J. Solid State Chem.* **5,** 354 (1972).
19. J. Berkowitz, W. A. Chupka, and M. G. Ingham, *J. Chem. Phys.* **27,** 85 (1957).